The magnetic properties of the quaternary intermetallic $GdNi_2B_2C$ and GdNiBC compounds

1995 J. Phys.: Condens. Matter 7 10015

(http://iopscience.iop.org/0953-8984/7/50/031)

J. Phys.: Condens. Matter 7 (1995) 10015–10027. Printed in the UK

The magnetic properties of the quaternary intermetallic $GdNi_2B_2C$ and GdNiBC compounds

M El Massalami†‖, B Giordanengo†, J Mondragon†, E M Baggio-Saitovitch†, A Takeuchi†, J Voiron‡ and A Sulpice§

† CBPF, Rue Xavier Sigaud 150, 22290-180, Rio de Janeiro, Brazil
‡ Laboratoire Louis-Néel, CNRS, Grenoble Cédex 09, France
§ CRTBT, CNRS, BP 166, 38042 Grenoble, France

Received 24 April 1995, in final form 30 October 1995

Abstract. The magnetic features of $GdNi_2B_2C$ ($I4/mmm$, $a = 3.578$ Å, $c = 10.361$ Å) and GdNiBC ($P4/nmm$, $a = 3.631$ Å, $c = 7.546$ Å) have been studied for 1.2 K $< T <$ 300 K and in fields up to 140 kOe. In both types of compound, the spherical ^8S state of the Gd^{3+} ion can be unambiguously observed in the features of the paramagnetic state as well as the low-T field-induced ferromagnetic state. The observed Néel points for $GdNi_2B_2C$ and GdNiBC are, respectively, 19.5(5) K and 14.3(5) K, and their magnetic structures at $T = 0$ are presumably the collinear Néel-type structures. The saturating field in $GdNi_2B_2C$ ($H \geqslant 125$ kOe at 1.7 K) is approximately three times that of GdNiBC implying that the average interlayer interactions in the former are much stronger than in the latter. The overall magnetic features of both compounds are interpreted in terms of the picture that assumes the Gd moments to have strong ferromagnetic intralayer couplings and averaged antiferromagnetic interlayer interactions.

1. Introduction

The basic structural building blocks of the chemically layered series $(RC)_m(NiB)_n$ where R = rare earth, Y; $(m, n) = (1, 1), (1, 2), (2, 1)$ are the rock-salt-type RC layer and the inverse PbO-type Ni_2B_2 layer [1, 2]: the structures of the compounds for various values of (m, n) differ only in their stacking patterns. The magnetism in this series [3, 4, 5, 6] is found to be governed solely by the magnetic moment of the square-coordinated R^{3+} ions, indicating that the tetrahedrally coordinated Ni ions have no magnetic contribution. In general, these structural features are found to give rise to various interesting magnetic properties. As an example, in the isomorphous intermetallics RNi_2B_2C (R = Tm, Er, Ho, Dy, Tb), the 4f moments have strong intralayer ferromagnetic (FM) couplings and relatively weak interlayer antiferromagnetic (AFM) interactions [3, 6]. The latter interactions are responsible for the magnetic ground state which plays a determinant role in the interplay between magnetism and superconductivity as demonstrated elegantly by neutron diffraction studies on $HoNi_2B_2C$ [4, 5].

It is interesting to investigate how the magnetic properties of the $(RC)_m(NiB)_n$ family evolve with the variation of the number of intercalated RC layers. In this work we present our studies on $GdNi_2B_2C$ and GdNiBC compounds. We have deliberately chosen R = Gd since the Gd ions are in the ^8S spherical state [6, 7, 8, 9], and therefore complications due to

‖ Present address: Instituto de Fisica—UFRJ, Caixa Postal 68528, 21945-970, Rio de Janeiro, Brazil.

0953-8984/95/5010015+13$19.50

crystal-field effects are avoided while the restriction to $(m, n) = (1, 1)$ and $(1, 2)$ is imposed due to the ease of preparing these compounds in a chemically pure and stable form.

The nonsuperconductor $GdNi_2B_2C$ [2] crystallizes in a body-centred tetragonal structure (space group $I4/mmm$) with an alternate stacking of Ni_2B_2 and GdC layers. Its magnetic ordering temperature ($T_N = 20$ K) is the highest among those of the magnetic members of the RNi_2B_2C series [1, 3, 6]. This is not surprising since, for this series, T_N is shown [3, 6] to scale with the de Gennes factor, $(g-1)^2J(J+1)$, and this factor is largest for the Gd ion. Its low-T magnetic structure is not yet elucidated. In this work, (magneto-) resistivity and high-field magnetization studies are employed in an attempt to deduce the overall features of its magnetic ground state.

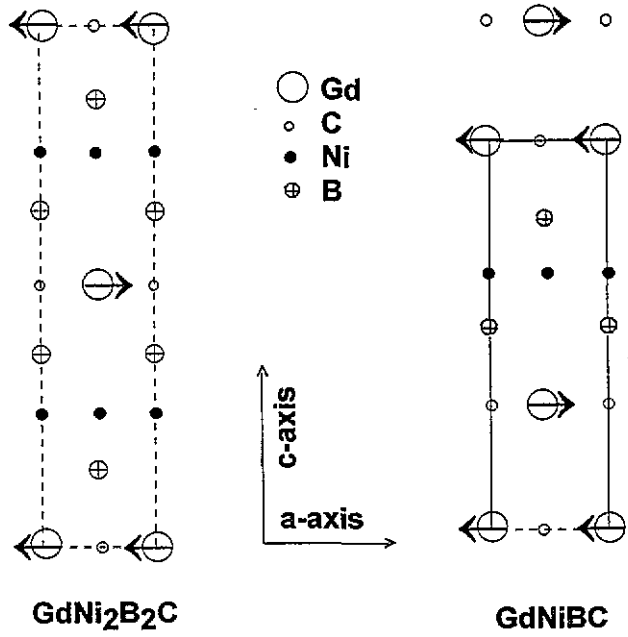

Figure 1. The ac-plane projection of the structural features and the magnetic ground state at $T = 0$ K of $GdNi_2B_2C$ and GdNiBC. The units cells are marked by dotted lines. The arrows indicate the orientations of the Gd moments.

On the other hand, the structural features of the GdNiBC compound (isomorphous to LuNiBC [2] and HoNiBC [10]) indicate that the Ni_2B_2 sheets are separated by double NaCl-type GdC layers (see figure 1). An insertion of an extra GdC layer into the structure of $GdNi_2B_2C$ (see figure 1) is expected to modify drastically the magnetic properties of the derived GdNiBC compound. In this work we describe our preliminary magnetic and resistivity studies which confirm this expectation.

Finally, the magnetic structures, as studied by neutron diffraction techniques, are available only for RNi_2B_2C, where R = Er, Ho, Dy [4, 5, 11, 12]. The low-T spin structure for R = Er is an incommensurate modulated AFM state with $Q = 0.553a^*$, while for R = Ho, Dy, it is a commensurate AFM state. It is highly possible that (due to energy minimization considerations) the low-temperature magnetic structures of $GdNi_2B_2C$ and GdNiBC are as sketched in figure 1: the FM layers are coupled into a collinear AFM structure. However, at intermediate temperatures, the magnetic structures of these layered compounds are not so obvious. In this work, an attempt is made to investigate their intermediate magnetic structures.

2. Experimental details

The samples were prepared and afterwards annealed according to the conventional argon arc-melting method [1, 2]. Room-temperature Cu Kα x-ray diffraction, and Rietveld refinement were used for the structural analysis. Magnetization measurements were carried out for the following set-ups: ac susceptibility (500 Hz, 1 Oe, 1.5 K $< T <$ 50 K); a SQUID magnetometer (1.7 K $< T <$ 100 K, $H <$ 80 kOe); and an extraction magnetometer (1.7 K $< T <$ 100 K, 0 $< H <$ 140 kOe). The dc four-point method was used for the (magneto-) resistivity measurements. In this work, no correction was made for the diamagnetic contribution or for form factors and, in addition, because of the combined effects of impurities and polycrystallinity, no attempt was made to estimate the spin-flop field in the high-field magnetization isotherms.

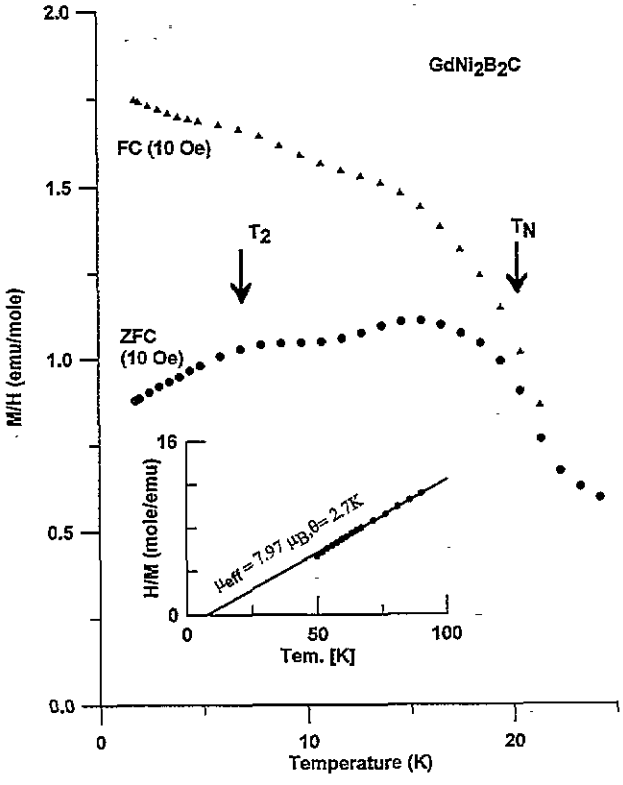

Figure 2. *M–T* curves (H = 10 Oe) of $GdNi_2B_2C$ showing the field-cooled (FC) and the zero-field-cooled (ZFC) behaviour. The inset shows the reciprocal of the dc susceptibility, $1/\chi_{dc}$, against T.

3. Results

3.1. $GdNi_2B_2C$

Preliminary results on this compound were reported in [7, 8]. Our structural analysis showed that the $GdNi_2B_2C$ is the major phase (93%) and the prime impurity phase was identified as GdNiBC. The structural parameters (see table 1) are in good agreement with the published results [2] and, together with the important Gd–Gd distances, are listed in table 1.

Table 1. Some structural parameters of GdNiBC and $GdNi_2B_2C$. Gd1–Gd1 denotes the separation between the intralayer nearest neighbours while Gd1–Gd2 and Gd1–Gd3 denote the separations between, respectively, the nearest and the next-nearest interlayer neighbours.

Compound	Space group	Gd-site symmetry	a (Å)	c (Å)	Gd1–Gd1 (Å)	Gd1–Gd2 (Å)	Gd1–Gd3 (Å)
GdNiBC	$P4/nmm$	$4mm$	3.631	7.546	3.631	3.577	7.546
$GdNi_2B_2C$	$I4/mmm$	$4/mmm$	3.578	10.361	3.578	5.765	10.361

For $T > 50$ K, the Curie–Weiss (CW) paramagnetism is characterized by $\mu_{eff} = 7.97\ \mu_B$ (the expected value is $7.937\ \mu_B$) and $\theta = +2.7$ K (figure 2). As the temperature is decreased, a set of magnetic transitions appear (figure 2). A weak peak at around 45 K is attributed to an unidentified magnetic impurity. It is highly possible that the hump at around 14 K is due to a small impurity in GdNiBC (see later). The two transitions that are intrinsic to $GdNi_2B_2C$ are: one peaking at around $T_N = T_1 = 19.5(5)$ K (attributed to an AFM transition); and another weak inflection in the χ_{dc}–T curve at $T_2 = 7.2(3)$ K (figure 2).

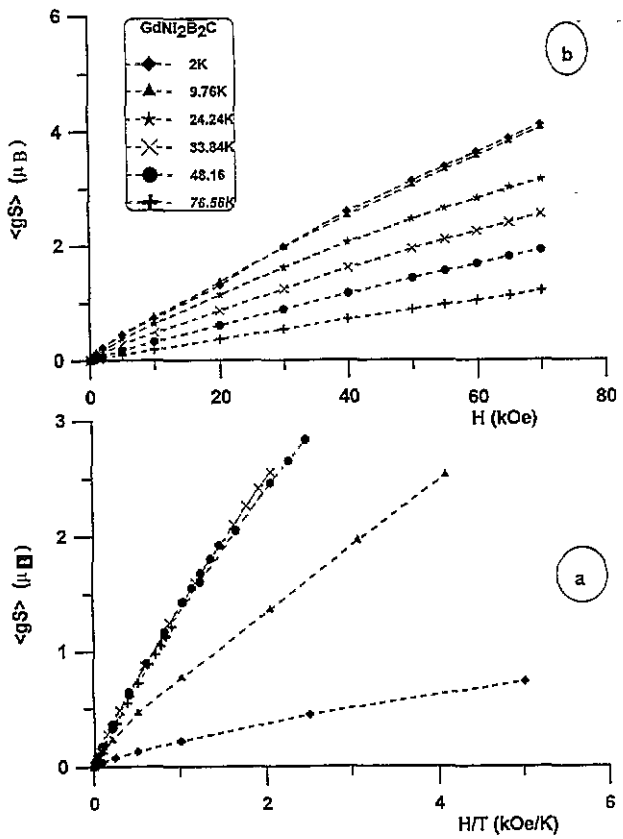

Figure 3. Magnetization isotherms of $GdNi_2B_2C$ at different temperatures. (a) M–(H/T) curves illustrating the difference between the ordered and the paramagnetic states (see the text). (b) M–H curves for different temperatures. $\langle\ldots\rangle$ denotes the thermally averaged value (g is the g-factor and S is the total orbital moment).

Magnetically layered $GdNi_2B_2C$ (see figure 1) can be investigated by the use of the molecular field (MF) treatment so as to roughly calculate the exchange interactions from T_N and θ. Let us assume only intralayer interactions J_1 (among Z_1 nearest neighbours) and interlayer interactions J_2 (among Z_2 neighbours). Then [13],

$$Z_1 J_1 - Z_2 J_2 = \frac{3T_N}{2S(S+1)} \tag{1}$$

$$-2Z_2 J_2 = \frac{3C}{\chi(T_N)2S(S+1)} \tag{2}$$

$$Z_1 J_1 + Z_2 J_2 = \frac{3\theta}{2S(S+1)} \tag{3}$$

where S (=7/2), C (=7.94 emu K mol^{-1}) and $\chi(T_N)$ ($\simeq$0.5 emu mol^{-1}) are the total angular momentum, the Curie constant and the molar susceptibility at T_N, respectively. Equations (1)–(3) yield $Z_1 J_1 = 1.1$ K and $Z_2 J_2 = -0.8$ K. Since the magnetic interactions are of a long-range type, Z_i does not represent the chemically neighbouring Gd ions. The negative sign of J_2 emphasizes the AFM character of the average interlayer interactions while the positive sign of J_1 and θ indicates that the dominant interactions are of FM character.

Below T_N, the field-cooled (FC) and the zero-field-cooled (ZFC) magnetization curves (figure 2) show that a fraction of the magnetization is remnant under even a 10 Oe magnetic field. This effect may be attributed to domain pinning on defects arising from a small amount (a few per cent) of atomic disorder (such as C deficiency or B–C site interchange) that are beyond our XRD diffraction resolution.

Figure 3 shows the magnetization isotherms at $T = 2$ K, 9.76 K, 24.23 K, 33.84 K, 48.16 K, 76.56 K. In the paramagnetic state ($T > \theta$), the M versus H/T curves should collapse to

$$M = \chi H = CH/(T-\theta) \approx CH/T. \tag{4}$$

This is confirmed in figure 3(a). In addition, figure 3(b) shows that, in the ordered state, the M–H curves at $T = 9.76$ K and $T = 2.0$ K are not different for higher fields. Furthermore, the high-field powder M–H curve at 1.7 K (figure 4) shows that the magnetic moment per Gd ion, $\langle gS \rangle$, rises rapidly at low field and then slowly up to 40 kOe. Above that, for 40 kOe $< H_{ap} <$ 100 kOe, the magnetization rises quasi-linearly:

$$\langle gS \rangle = (0.055 H_{ap} + 0.79)\ \mu_B. \tag{5}$$

For $H \geqslant H_{sat} = 125(5)$ kOe, the saturated moment is 7.13 μ_B (the expected value is 7 μ_B). The excess moment (0.13 μ_B) is most probably due to the contaminating magnetic phases since, in the magnetic members of RNi_2B_2C, no magnetic contribution from the Ni ions was found. The high value of the saturation field stressed the fact that the magnetic interactions in $GdNi_2B_2C$ are extremely strong. This fact is convincingly demonstrated by the M–H curve of $(Gd_{0.2}Y_{0.8})Ni_2B_2C$ (see the inset of figure 4) where 80% of Gd ions have nonmagnetic Y ions substituted for them [7, 8]. In spite of this drastic magnetic dilution, the magnetic saturation at $T = 1.6$ K in $(Gd_{0.2}Y_{0.8})Ni_2B_2C$ is achieved only for $H > 70$ kOe.

The resistivity (figure 5) reveals a metallic behaviour down to 30 K and, for $T_N < T <$ 30 K, ρ shows T-independent saturation features. Below T_N, a drop in the resistivity is observed, which is obviously related to the onset of the long-range magnetic order.

3.2. *GdNiBC*

Our XRD structural analysis showed that the GdNiBC is a tetragonal compound with space group $P4/nmm$. The lattice parameters and the relevant Gd–Gd distances are given in

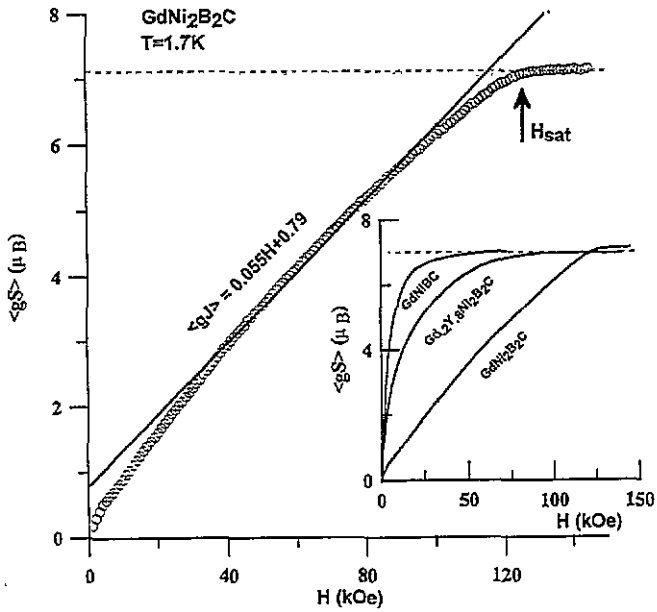

Figure 4. The M–H curve at 1.7 K for $GdNi_2B_2C$. The continuous line is a fit to the MF predictions for a weakly anisotropic Heisenberg AFM (see the text). The inset compares the magnetization isotherms for $GdNi_2B_2C$ (T = 1.7 K), $(Gd_{0.2}Y_{0.8})Ni_2B_2C$ (T = 1.6 K) and GdNiBC (T = 4.2 K).

table 1. Traces of impurity phases were detected (<5%) and the prime contaminating phase was identified as $GdNi_2B_2C$.

The magnetic susceptibility measurements (figure 6) show a CW behaviour down to approximately 45 K. The CW parameters obtained are: $\mu_{eff} = 7.94\ \mu_B$ and $\theta = 23.8(4)$ K. A remarkable deviation from the CW behaviour starts to be evident below 45 K (see later). Furthermore, figure 6 shows clearly that the long-range magnetic order sets in at $T_N = 14.3(5)$ K and is of an AFM character. As can be deduced from table 1 and figure 1 (see figure 9 later), on the insertion of an additional GdC layer in $GdNi_2B_2C$, the intralayer separations (intralayer interactions) are slightly modified while the interlayer separations (interlayer interactions) are drastically changed. If, then, Z_1J_1 are considered to be similar in the two compounds, the average interlayer interaction of GdNiBC, Z_2J_2, is −0.28 K: one third of the corresponding value for $GdNi_2B_2C$.

Table 2. Some magnetic parameters of GdNiBC and $GdNi_2B_2C$.

Compound	μ_{sat} (μ_B)	μ_{eff} (μ_B)	T_N (K)	θ (K)	H_c (kOe)
GdNiBC	7.0	7.94	14.3(5)	23.8(4)	≃40
$GdNi_2B_2C$	7.13	7.97	19.5(5)	2.7	125(5)

The field response of the AFM state is indicated by the magnetization isotherm at $T = 4.2$ K (see figure 7). The magnetization increases monotonically with the applied field until saturation is attained for $H > 40$ kOe. As is evident from table 2, the saturation field is approximately one third of the value found for $GdNi_2B_2C$.

The resistivity (figure 8) shows a metallic behaviour in the high-T regime. Below 100 K,

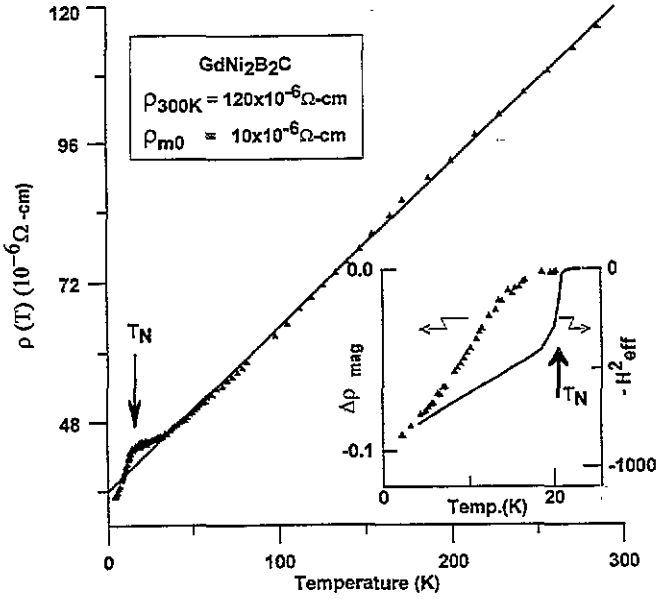

Figure 5. The room-temperature normalized resistivity versus temperature for $GdNi_2B_2C$. The inset shows the influence of the magnetic ordering on the resistivity below T_N; the continuous line is the square of the sublattice magnetization as given by Mössbauer spectroscopy ($M(T) \propto H_{eff}(T)$) [9].

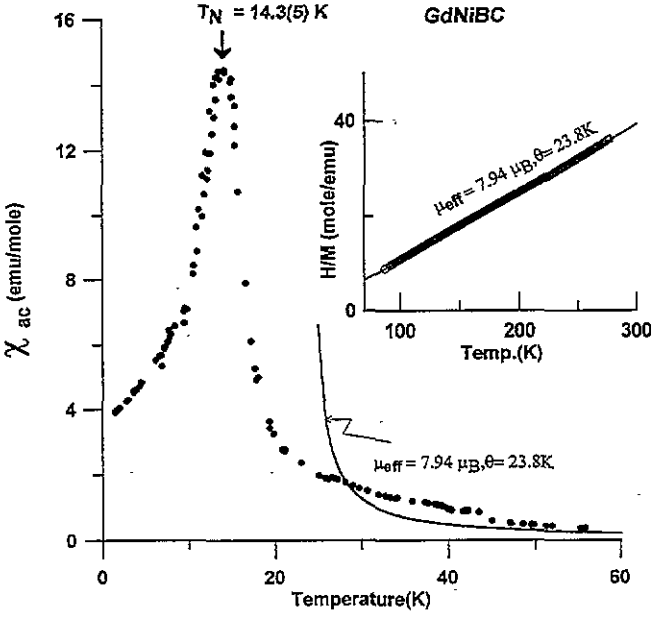

Figure 6. The magnetic susceptibilities of GdNiBC. The inset demonstrates the Curie–Weiss features of GdNiBC.

ρ starts to deviate from the linear behaviour and reaches a minimum at around 50 K and then increases monotonically as the temperature is decreased down to T_N. Below T_N, the long-range magnetic order causes a steady drop in the ρ–T curve and with no sign of saturation

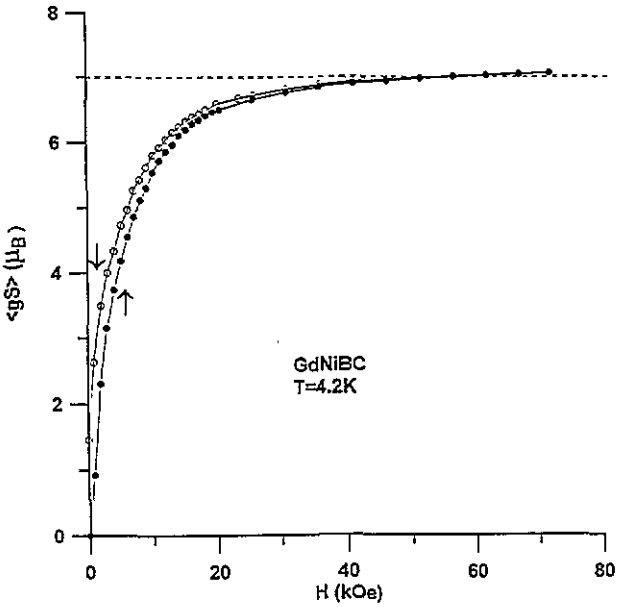

Figure 7. The M–H curve at $T = 4.2$ K for GdNiBC. The small hysteresis effects may be attributed to lattice imperfections.

down to the lowest measured temperature. Both anomalies (in the ρ–T curve (figure 8) and in the χ_{dc}–T curve (figure 6)) are found to be sensitive to the sample preparation route and may be due to short-range ordering or magnetic fluctuations accompanying the AFM order. It is less likely that these features arise solely from magnetic impurities (having $T_N \approx 45$ K and $T_N = 20$ K) since, if there are sizable magnetic impurities to the extent that they give rise to such a deviation from the CW law, then the ordering of these impurities is expected to induce a decrease (and not an increase) in the net ρ_m.

4. Discussion

In the paramagnetic phase, θ reflects the dominant intralayer interactions while the strength of T_N is largely determined by the interlayer couplings. It is an experimental fact that in RNi_2B_2C (R = Tm, Ho, Dy, Gd), T_N can be scaled to $(g-1)J(J+1)$, while θ cannot. Therefore, it is tempting to infer that the interlayer interactions in these compounds are of RKKY type while the intralayer interactions, in addition, include a superexchange-type (mediated through the carbon ions) component. The RKKY-type interaction is usually written as [15, 16, 17]

$$J(R_{ni}) = \frac{9\pi n^2 \Gamma^2 (g-1)^2}{8V^2 \epsilon_F} F(2k_F R_{ni}) \exp(-R_{ni}/\lambda)$$
$$F(x) = \left[\frac{x\cos(x) - \sin(x)}{(x)^4}\right] \tag{6}$$

and the paramagnetic spin-disorder resistivity, ρ_{m0}, is

$$\rho_{m0} = \frac{\hbar k_F}{4\pi n V}\left(\frac{m^*\Gamma}{e\hbar^2}\right)^2 (g-1)^2 S(S+1) \tag{7}$$

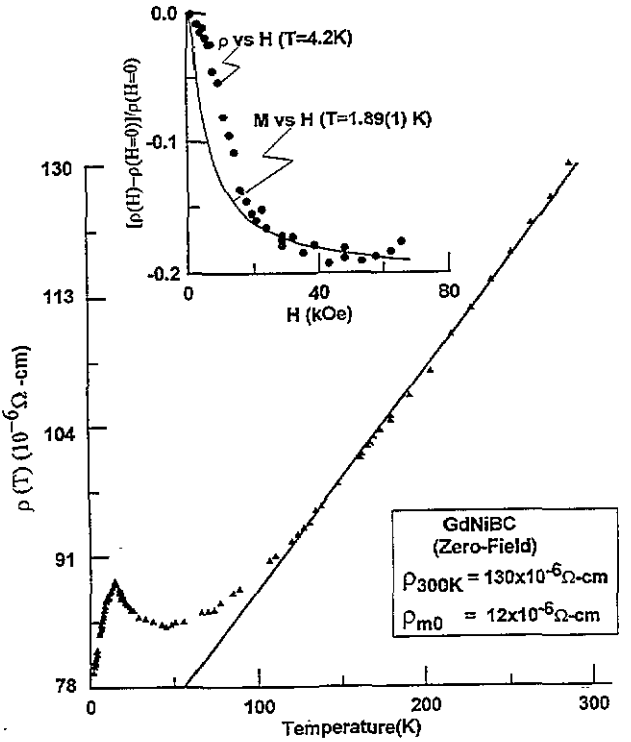

Figure 8. *The room-temperature normalized resistivity versus temperature for GdNiBC. The* inset scales $\Delta\rho(H)$ ($T = 1.89$ K) with $M^2(H)$ ($T = 4.2$ K), assuming that $M(H)$ at 4.2 K is not drastically different from that at $T = 1.89$ K.

where Γ is the s–f exchange coupling ($\sim$1 eV Å^3), n (1.1×10^{22}) is the carrier concentration, R_{ni} is the distance separating two Gd moments, ϵ_F (0.38 eV) and k_F ($\sim 0.32 \times 10^8$ cm^{-1}) are the Fermi energy and wave vector [18, 19] and λ ($> R$) is the mean free path. For $GdNi_2B_2C$ (to which also belong the bracketed numerical values), equation (7) gives $\rho_{m0} \approx 6 \times 10^{-6}$ Ω, in fair agreement with the experimental values (see figure 5) and, from equation (6), the interlayer interactions $J(R_{n1} = 5.765$ Å$) = -1.1$ K (in good agreement with Z_2R_2-values found from equations (1)–(3)) and $J(R_{n2} = 10.361$ Å$) = 0.25$ K. The sinusoidal character of $J(2k_F R_{ni})$ is plotted in figure 9 as a function of the separating distances along the c-axis.

It is worth mentioning that for $GdNi_2B_2C$, $J(R_{n1})/J(R_{n2}) \approx -4.4$, which is not far from satisfying the condition for the onset of the helimagnetic spin arrangement [15] ($|J(R_{n1})/J(R_{n2})| < 4$). In fact our susceptibility data (figure 2) suggest a second (though weak) magnetic transition at $T_2 = 7.2(3)$ K. So far there are no experimental studies that evaluate directly the magnetic structure of $GdNi_2B_2C$ below T_N. Nevertheless, this transition can be qualitatively interpreted if we assume (in analogy with the magnetic features of $HoNi_2B_2C$ [1, 3]) that the ordering at $T_N = 20$ K is accompanied by an incommensurate component that transforms to a commensurate AFM state at $T_2 = 7.2(3)$ K. In contrast, in GdNiBC, the uneven spacing of the magnetic layers along the c-axis makes it impossible to sustain a constant spiral angle between the moment orientations of adjacent FM sheets, and so no helical state will be expected.

The MF analysis of the previous section is expected to hold since it does not depend on the specific nature of the magnetic interactions. In general, these space-dependent

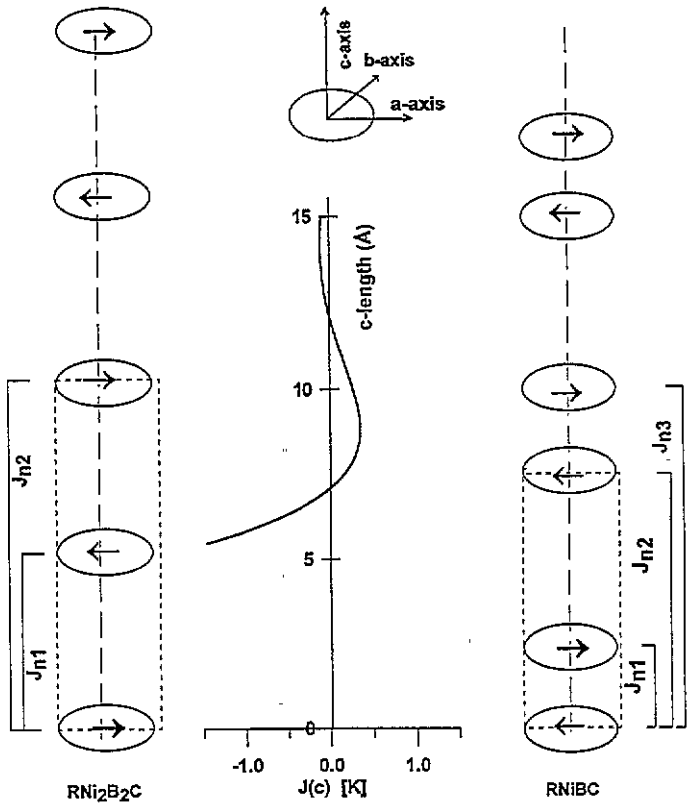

Figure 9. A schematic representation of the interlayer magnetic bonds in the layered compounds $GdNi_2B_2C$ and GdNiBC (J_{ni} is the coupling among the nth and $(n+i)$th layers). The unit cells are represented by dotted rectangles while the ferromagnetic planes (perpendicular to the c-axis) are represented by discs. The middle curve is a plot of $J(c)$ as a function of the separating distance along the c-axis. If the interactions are restricted to only the first- and second-nearest neighbours, this gives the so-called three-layer exchange model [15].

interactions dictate the strength of $H_{sat}(H_{ex})$, T_N and θ. Thus it is not surprising that $H_{sat}(H_{ex})$, T_N and θ are different for GdNiBC and $GdNi_2B_2C$ (see table 2). However, what is really surprising is that both H_{sat} and T_N for GdNiBC are systematically lower than those for $GdNi_2B_2C$. This is contrary to what is generally expected: on increasing the magnetic dimensionality of the system these parameters should increase (GdNiBC is a step towards the fictitious three-dimensional limit compound GdC). It is remarkable that θ follows the expected trend (see table 2).

This lowering of H_{sat} and T_N in GdNiBC as compared to in $GdNi_2B_2C$ can only be due to the variation in the interlayer interactions since, as mentioned above, the intralayer couplings are considered to be quasi-equal in the two compounds. The intercalation of extra GdC layers involves the creation of additional magnetic bonds (see figure 9) that may have opposite and competing tendencies for magnetic ordering. Such competition may lead to the lowering of the interlayer interactions and to a thermally assisted magnetic frustration which are manifested as an increase in the spin-disorder resistivity and also as an anomalous deviation from CW law well above T_N. Frequency-dependent susceptibility and ^{151}Gd Mössbauer spectroscopy studies are under way to test this proposition.

Now let us discuss the field response of the low-T AFM structures of both compounds. It is mentioned above that the single-ion magnetic anisotropy in both compounds is negligibly small (see table 1 for the point symmetry at the Gd site). Moreover, the magnetic interactions are expected to be isotropic. Thus, $GdNi_2B_2C$ and GdNiBC can be considered as (weakly anisotropic) Heisenberg AFMs and, within the MFA, the magnetization isotherms for $T < T_N$ can be described as follows [13, 14]:

$$M/M_s = H_{ap}/(2H_{ex} - H_a) \approx H_{ap}/2H_{ex} \tag{8}$$

$$H_{sat} = (2H_{ex} - H_a) \approx 2H_{ex} \tag{9}$$

$$H_{sf} = \sqrt{2H_aH_{ex} - H_a^2} \approx 0 \tag{10}$$

where, H_{ex}, H_a, H_{sat} and H_{sf} are, respectively, the exchange field, the anisotropy field ($\ll 2H_{ex}$), the saturation field and the spin-flop field. M_s is the sublattice magnetization ($\frac{1}{2}Ng\mu_B J$). These relations are valid only for single crystal and, if polycrystalline results are desired, they must be integrated over the angular variables, in which case the sharp behaviour of the spin-flop transition will be smeared out. In this work, equations (8)–(10) are applied only for obtaining a qualitative understanding of the general field response features of the AFM state. As is evident, the qualitative features of the M–H curves of $GdNi_2B_2C$ (figure 4) and GdNiBC (figure 7) are in accord with these equations: the external field first flops the spins to the perpendicular direction (from equation (10) $H_{sf} \approx 0$) and afterwards works to align them parallel to the field against the AFM interlayer couplings. Complete moment saturation is achieved only when the exchange field is completely counterbalanced. For the case of $GdNi_2B_2C$, equation (8) is fitted to the M–H curve of figure 4 over the range 40 kOe $< H_{ap} <$ 100 kOe and the calculated H_{sat} ($H_{sat} = 2H_{ex} - H_a \approx 2H_{ex} = 127(7)$ kOe) agrees with the experimentally determined $H_{sat} = 125(5)$ kOe, in full agreement with equation (9). Moreover, the MFA estimate for the average exchange interaction is [13]

$$H_{ex} = 2\frac{k_B}{g\mu_B}\langle S\rangle|Z_2J_2|. \tag{11}$$

The derived average exchange interactions are in fair agreement with those of equations (1)–(3) and that for $GdNi_2B_2C$ (1.2 K) is three times larger than that for GdNiBC (0.39 K).

Although, the MF treatment has self-consistently succeeded in estimating the exchange interactions from the experimental parameters (equations (1)–(3), (6), (11)) and gave a reasonable value for ρ_{m0} (equation (7)), it fails to account for the thermal and field dependence of the resistivity of these compounds. This will be demonstrated by the T-dependent $\rho(T, H = 0)$ ($T < 20$ K) for $GdNi_2B_2C$ and the H-dependent $\rho(T = 1.8$ K, $H)$ for GdNiBC. The MFA connects $\Delta\rho$ to the thermally averaged Gd moment $\langle S\rangle$ [15]:

$$\Delta\rho = \frac{\rho_m(T, H) - \rho_{m0}}{\rho(0)} = -\langle S\rangle^2\alpha - \langle M\rangle^2 \tag{12}$$

where $\rho_m = \rho_{tot} - \rho_{ph} - \rho_{res}$ and ρ_{ph} and ρ_{res} are, respectively, the resistivity as contributed by the phonon and that from the lattice imperfections. For $GdNi_2B_2C$, the inset of figure 5 demonstrates the relation between the normalized magnetic resistivity $\Delta\rho$ and the sublattice magnetization, M, as measured by ^{151}Gd Mossbauer spectroscopy [9] where M is proportional to the effective hyperfine field, H_{eff}. The inset shows that while $-H_{eff}^2$ drops very fast below T_N and slowly afterwards, $\Delta\rho$ drops with a much slower rate. No doubt the trend is similar; however, the fact that $\Delta\rho$ does not scale well with $\langle S\rangle^2$ implies that the MF approximation is not applicable in this case.

For GdNiBC, the feature of normalized longitudinal magnetoresistivity (see the inset of figure 8) shows that the magnetic contribution to the resistivity decreases monotonically with H until magnetic saturation is attained. For comparison, the experimentally determined M–H curve at 4.2 K (figure 7) is substituted into equation (12) and plotted together with $\Delta\rho$ at 1.89 K in the inset of figure 8. As is evident, the failure of scaling $\langle M\rangle^2$ with $\Delta\rho(H)$ indicates, once more, that the MFA relation (equation (12)) is not appropriate for the description of the magnetoresistivity behaviour of these compounds.

5. Conclusion

The quaternary intermetallic conductors $GdNi_2B_2C$ and GdNiBC show high-T paramagnetism and low-T field-induced ferromagnetism which are compatible with a Gd^{3+} ionic state. Their magnetic features are dictated by strong FM intralayer interactions and (averaged) AFM interlayer couplings and the low-T magnetic ground states are expected to be the commensurate AFM structures.

MF treatment shows that GdNiBC ($T_N \approx 14.3$ K, $H_{sat} \approx 40$ kOe) is characterized by relatively lower interlayer interactions than those of $GdNi_2B_2C$ ($T_N \approx 20$ K, $H_{sat} \approx 125$ kOe), even though the presence of additional GdC layers in its structure is expected to enhance its three-dimensional magnetic character and thus increase T_N and H_{sat}. Furthermore, GdNiBC shows two additional anomalies: a deviation from CW behaviour in the χ_{dc}–T curve and an anomalous rise in the ρ–T curve just above T_N. Both features are evident at temperatures as high as $3T_N$ and are found to be sensitive to the sample preparation route. These anomalous features of GdNiBC are tentatively attributed to possible short-range order effects or magnetic frustration that may be arising from the presence of opposing coupling tendencies in the interlayer interactions.

The magnetoresistive properties of the two compounds do not compare favourably with the simple MFA. Finally, in contrast to those of the RNi_2B_2C compounds, the structural features of GdNiBC, with its non-uniform spacing of magnetic layers along the c-axis, exclude the possibility of sustaining an incommensurate state at an intermediate range of temperatures.

Acknowledgments

We acknowledge the fruitful discussions with and critical reading by Professor M A Continentino and H Micklitz. Experimental help from R Pereira is gratefully acknowledged.

References

[1] Cava R J, Takagi H, Batlogg B, Zandbergen H W, Krajewski J J, Peck W F Jr, Siegrist T, van Dover R B, Felder R J, Mizuhashi K, Lee J O, Eisaki H and Uchida S 1994 *Nature* **367** 252

[2] Siegrist T, Zandbergen H W, Cava R J, Krajewski J J and Peck W F 1994 *Nature* **367** 254
Zandbergen H W, Cava R J, Krajewski J J and Peck W F Jr 1994 *Physica* C **224** 6
Siegrist T, Cava R J, Krajewski J J and Peck W F Jr 1994 *J. Alloys Compounds* **216** 135

[3] Eisaki H, Takagi T, Cava R J, Mizuhashi K, Lee J O, Batlogg B, Krajewski J J, Peck W F Jr and Uchida S 1994 *Phys. Rev.* B **50** 647

[4] Grigereit T E, Lynn J W, Huang Q, Santoro A, Cava R J, Krajewski J J and Peck W F Jr 1994 *Phys. Rev. Lett.* **73** 2756
Huang Q, Santoro A, Grigereit T E, Lynn J W, Cava R J, Krajewski J J and Peck W F Jr 1995 *Phys. Rev.* B **51** at press

[5] Goldman A I, Stassis C, Canfield P C, Zarestky J, Dervenagas P, Cho B K and Johnston D C 1995 *Phys. Rev.* B **50** 9668
[6] El Massalami M, Bud'ko S L, Giordanengo B and Baggio-Saitovitch E M 1995 *Physica* C **244** 41
[7] El Massalami M, Bud'ko S L, Giordanengo B, Fontes M B, Mondragon J C and Baggio-Saitovitch E M 1994 *Physica* C **235–240** 2563
[8] El M Massalami, Bud'ko S L, Giordanengo B, Fontes M B, Mondragon J C and Baggio-Saitovitch E M 1995 *Phys. Status Solidi* b **189** 489
[9] Mulder F M, Brabers J V V J, Cochoorn R, Thiel R C, Buschow K H J and de Boer F R 1995 *J. Alloys. Compounds* **217** 118
[10] El Massalami M and Baggio-Saitovitch E M 1995 *J. Alloys. Compounds* **228** 49
[11] Sinha S K, Lynn J W, Grigereit T E, Hossain Z, Gupta L C, Nagarajan R and Godart C 1995 *Phys. Rev.* B **51** 681
Zarestky J, Stassis C, Goldman A I, Canfield P C, Dervenagas P, Cho B K and Johnston D C 1995 *Phys. Rev.* B **51** 678
[12] Dervenagas P, Zarestky J, Stassis C, Goldman A I, Canfield P C and Cho B K 1995 *Physica* B **212** 1
[13] Smart J S 1966 *Effective Field Theories of Magnetism* (New York: Saunders) p 101; 1963 *Magnetism III* ed G Rado and H Suhl (London: Academic) p 63
[14] Carlin R L and van Duyneveldt A J 1978 *Magnetic Properties of Transition Metal Compounds* (New York: Springer) p 184
[15] Coqblin B 1977 *The Electronic Structure of Rare-Earth Metals and Alloys: the Magnetic Heavy Rare-Earth* (London: Acadamic)
[16] Rocher Y A 1963 *Adv. Phys.* **11** 233
[17] Mattis D C 1965 *The Theory of Magnetism* (New York: Harper & Row) p 195
[18] Mattheiss L F 1994 *Phys. Rev.* B 13 279
[19] Pickett W E and Singh D J 1994 *Phys. Rev. Lett.* **72** 3702